



Reduced aggregation and sedimentation of zero-valent iron nanoparticles in the presence of guar gum

Alberto Tiraferri^a, Kai Loon Chen^b, Rajandrea Sethi^a, Menachem Elimelech^{b,*}

^a DITAG – Dipartimento di Ingegneria del Territorio, dell'Ambiente e delle Geotecnologie, Politecnico di Torino, Corso Duca degli Abruzzi, 24, 10129, Torino, Italy

^b Department of Chemical Engineering, Environmental Engineering Program, Yale University, New Haven, CT 06520-8286, USA

ARTICLE INFO

Article history:

Received 24 December 2007

Accepted 29 April 2008

Available online 7 May 2008

Keywords:

Zero-valent iron nanoparticles

Guar gum

Green polymers

Aggregation

Steric stabilization

Groundwater remediation

DLS

Particle size

ABSTRACT

Injection of nanoscale zero-valent iron (NZVI) is potentially a promising technology for remediation of contaminated groundwaters. However, the efficiency of this process is significantly hindered by the rapid aggregation of the iron nanoparticles. The aim of this study was to enhance the colloidal stability of the nanoparticles through the addition of the “green” polymer guar gum. We evaluated the properties of guar gum and its influence on the surface properties, particle size, aggregation, and sedimentation of iron nanoparticles. Commercial iron nanoparticles were dispersed in guar gum solutions, and their aggregation and sedimentation behaviors were compared to those of bare iron nanoparticles and commercial nanoparticles modified with a biodegradable polymer (polyaspartate). High performance size exclusion chromatography, charge titration, and viscosity assessment showed that guar gum is a high molecular weight polymer which is nearly neutrally charged, rendering it suitable for steric stabilization of the iron nanoparticles. Electrophoretic mobility measurements demonstrated the ability of guar gum to adsorb on the nanoparticles, forming a slightly negatively charged layer. Dynamic light scattering experiments were conducted to estimate the particle size of the different nanoparticle suspensions and to determine the aggregation behavior at different ionic strengths. Guar gum effectively reduced the hydrodynamic radius of the bare nanoparticles from 500 nm to less than 200 nm and prevented aggregation of the nanoparticles even at very high salt concentrations (0.5 M NaCl and 3 mM CaCl₂). Sedimentation profiles of the different nanoparticle suspensions confirmed the improved stability of the iron nanoparticles in the presence of guar gum. The results strongly suggest that guar gum can be used to effectively deliver stabilized zero-valent iron nanoparticles for remediation of contaminated groundwater aquifers.

© 2008 Elsevier Inc. All rights reserved.

1. Introduction

Groundwater remediation technologies, in particular for non-aqueous phase liquids (NAPL) contamination, have undergone a period of significant advancement when focus has shifted from ex situ systems to less invasive in situ techniques, such as permeable reactive barriers [1,2] and in situ enhanced natural attenuation [3]. However, these technologies usually do not provide efficient NAPL source zone remediation and often encounter engineering limitations related to the treatment depth, monitoring, and system construction. More recently, the use of nanoscale zero-valent iron (NZVI) has been studied to overcome these restrictions and several investigations have been undertaken to study specific targeting of the NAPL phase based on delivering agents with preferential affinity for the target zone [4]. With its small size and high specific surface area, NZVI should enable high reactivity [5] and subsurface

mobility for direct, non-invasive treatment of contaminated subsurface sites.

Several studies reported the efficiency of NZVI to react with halogenated organic solvents [6–9], pesticides [10,11], PCBs [12,13], PAHs [14], and a variety of metal ions [15], including As(III) [16,17], Cr(VI), and Pb(II) [18]. Other field tests have demonstrated the potential of NZVI for in situ remediation [7,19,20]. Nevertheless, high reactivity of NZVI alone is not sufficient to ensure effective remediation. To date, there is still uncertainty regarding the technology's potential for full-scale field application. Furthermore, no consensus has been reached on a number of fundamental issues, including NZVI stability, mobility, and longevity under subsurface conditions. To be effective for in situ subsurface remediation, NZVI particles must be stable to aggregation and have a very low deposition (or filtration) rate, as otherwise their mobility in the subsurface will be greatly limited [21,22]. In addition, aggregation will result in a decrease in the NZVI specific surface area which, in turn, would affect its reactivity.

Surface modification of the iron nanoparticles can both decrease the affinity to soil grain surfaces and increase colloidal

* Corresponding author. Fax: +1 203 432 2881.

E-mail address: menachem.elimelech@yale.edu (M. Elimelech).

stability, thus enhancing the mobility in the subsurface [23]. The propensity of NZVI to rapidly form aggregates of large size is to a large extent attributable to long-ranged attractive magnetic forces between the particles [24]. In order to ensure proper remediation, strong long-ranged repulsive forces are needed to overcome this magnetic attraction between the iron nanoparticles. Electrostatic stabilization, which is sensitive to ionic strength and composition, is unlikely to be effective. Another option is to pre-coat the iron nanoparticles with hydrophilic polymers whose long loops and tails extend out into solution, leading to steric stabilization. Systems that are sterically stabilized tend to remain well-dispersed even under conditions where the zeta potential of the surfaces is significantly reduced [25]. Furthermore, steric stabilization is effective at both high and low solid contents. Recent studies on polymer coating of nanoparticles have shown promising results. Investigations of NZVI stability and mobility in porous media have been carried out using anionic carbon [22], polyacrylic acid [22,26], starch [27], oil-based microemulsions [20], and anionic copolymers [4]. However, some of the previously studied modifiers are expensive and, therefore, would not be economical for large-scale applications.

Ideally, modified NZVI nanoparticles should be inexpensive, simple for use, and have no adverse impact on the environment. The twelve principles of green engineering [28] promote the use of material and energy inputs that are as inherently non-hazardous as possible, with inputs that are renewable as opposed to depleting. The above principles also have to accommodate requirements of mass, energy, space, and time efficiency. The present study adheres to the above principles. In addition to the desire to improve technological and environmental performance, our choice of surface modifiers was mindful of the implications that rest beyond the simple engineering requirement for NZVI nanoparticle stabilization.

The objective of this study is to assess the suitability of inexpensive, commercially available and green (of natural origin) polymers for use as stabilizing agents for iron nanoparticles. Specifically, we compared alginate, potato starch, and guar gum for their effectiveness in stabilizing iron nanoparticles. We have shown that guar gum is the most effective polymer for long-term stabilization of the nanoparticles. Consequently, the effect of guar gum on commercially available reactive zero-valent iron nanoparticles was studied in greater detail. The size, aggregation behavior, and sedimentation rate of the nanoparticles in the presence of guar gum were determined under different solution chemistries. Results were compared to those obtained with commercially available bare nanoparticles and sodium polyaspartate-coated nanoparticles. Guar gum demonstrated the capability to effectively coat the iron nanoparticles creating a slightly negatively charged layer. More importantly, guar gum has the ability to stabilize the iron nanoparticles through steric repulsion, as evidenced by the smaller particle size as well as the reduced aggregation and sedimentation.

2. Materials and methods

2.1. Commercial iron nanoparticle dispersions

Commercial reactive bare iron nanoparticles (RNIP) were supplied by Toda Kogyo Corp. (Onoda, Japan), and were used as received or modified as described below. The chemical and physical properties of RNIP, as well as their synthesis procedure, have been described in other studies [8,24,29]. The RNIP were stored in deionized water at pH 11 at a concentration of approximately 300 g/L. Commercial RNIP modified with a biodegradable polymer was also supplied by Toda Kogyo Corp. According to the supplier, the polymer is sodium polyaspartate with a molecular weight of 2–3 kDa. These nanoparticles, denoted as RNIP-10AP, were stored

in aqueous solution (pH ~10.5) at a particle concentration of approximately 250 g/L. Polyaspartate, a biopolymer with carboxylic functional groups [30], is present in the RNIP-10AP suspension at a concentration of 4 wt% [31]. Prior to each experiment, a portion of these slurries was diluted in deionized water (Millipore) to obtain a 3 g/L stock suspension, which was subsequently shaken for 1 min and then sonicated (Aquasonic Model 150T, VWR Scientific Products, Pennsylvania) for 30 min to break up the large aggregates formed during storage. The suspensions for the various experiments were obtained from this stock. The concentration of nanoparticles in the suspensions was determined through gravimetric analysis. All the experiments were conducted at pH 7.0 ± 0.3 and at room temperature (23 °C).

Bare RNIP and RNIP-10AP were characterized using transmission electron microscopy (TEM) (Tecnai 12 Biotwin, FEI Company, Oregon) and dynamic light scattering (DLS) for particle sizing. For TEM analysis, the stock suspensions were diluted 1000 times and a drop of the diluted suspensions was placed on top of the carbon-coated grid and air-dried before inspection.

2.2. Screening of polymers for nanoparticle stabilization

Three different green biopolymers were used for initial screening. In addition to the commercial sodium polyaspartate-coated particles, our investigations included potato starch purchased from Acros (Geel, Belgium), alginate from brown algae (12–80 kDa), and guar gum. Both alginate and guar gum were supplied by Sigma Aldrich (St. Louis, MO). The polymers were evaluated through a sedimentation assessment of the nanoiron suspensions at high particle concentration in the presence of 1 mM NaCl. Polymer stock solutions were introduced into nanoparticle stock suspensions contained in glass vials to result in suspensions comprising iron nanoparticles (1.5 g/L) and polymers at five different concentrations (0, 0.13, 0.2, 0.27 and 0.4 wt%). The vials were sonicated for 1 min just prior to the sedimentation experiment. Digital photographs of the vials were taken at different times to qualitatively assess the rate of sedimentation and nanoparticle stability.

2.3. Preparation and characterization of guar gum solutions

2.3.1. Charge titration

Although pure guar gum is an uncharged polysaccharide, the actual charge density of the commercial polymer we used was determined by potentiometric titration. The guar gum solution was prepared at 100 mg/L concentration and was filtered through a 0.45 μm membrane filter. Total organic carbon (TOC) measurements (TOC-V CSH, Shimadzu, Kyoto, Japan) were carried out for guar gum solutions yielding 0.31 mg TOC per mg of guar gum. The automatic titrator employed for charge titration was a 794 Basic Titrino (Metrohm, Switzerland). The titrant (0.1 M NaOH) was added to the sample solution without background electrolyte. Prior to the experiments, the sample was acidified with 1.0 M HCl to pH 2.97. During titration, N_2 gas was introduced continuously into the sample solution to maintain a CO_2 -free environment. Blank titration was performed using a polymer-free solution under conditions identical to those used during the sample titration. The carboxylic acidity of guar gum was determined by comparing the amount of NaOH required to raise the pH of the guar gum solution from 3 to 10 with that required to raise the pH of a blank solution.

2.3.2. Viscosity

The viscosity of guar gum solutions was measured with a rheometer (AR 2000ex, TA Instruments, New Castle, DE) over a range of guar gum concentrations (0.05–1 g/L) and ionic strengths (1 mM NaCl, 10 mM NaCl, 0.5 M NaCl, and 3 mM CaCl_2). The measurements were carried out over a cycle of temperature variation

($25 \pm 0.1^\circ\text{C}$ to $5 \pm 0.1^\circ\text{C}$ to $25 \pm 0.1^\circ\text{C}$ to $45 \pm 0.1^\circ\text{C}$ to $25 \pm 0.1^\circ\text{C}$). A cone-and-plate geometry was employed using a 6 cm diameter cone with a 1° slope, and a Peltier plate was used for temperature control. The solutions were assumed to be Newtonian-like fluids. This assumption is accurate given that the viscosity was observed to be independent of the shear strain rate, i.e., the plot of shear strain rate against shear stress was always linear and passing through the origin.

The values obtained from viscosity measurements were used to derive the hydrodynamic radius of the nanoparticle aggregates obtained from DLS measurements (to be discussed in later sections), in which the size of the particles is related to the viscosity of the solution by

$$a = \frac{kT}{6\pi\eta D}, \quad (1)$$

where a is the hydrodynamic radius of the particles, η the viscosity of the solution, D the diffusion coefficient, k the Boltzmann constant, and T the absolute temperature of the solution.

2.3.3. Determination of molecular weight (MW)

High performance size exclusion chromatography with laser light scattering detector (DAWN®-EOS, Wyatt Technology, Santa Barbara, CA) was employed to measure the molecular weight of guar gum. Two samples were prepared at 0.5 g/L guar gum concentration at an unadjusted pH of approximately 6 before being filtered with a $0.45\ \mu\text{m}$ membrane filter. One of the two samples was sonicated using an Aquasonic Model 150T (VWR Scientific Products, Pennsylvania) for 30 min before the experiment. The system comprised a PWXL guard column to provide a first separation and protect the columns, followed by TSK6000 and 4000 columns. The gel permeation separation was carried out at room temperature using 0.1 M NaNO_3 as the eluent. Samples of the guar solutions (500 μL) were injected into the size exclusion system. Data were captured and analyzed using the software package ASTRA, and the molecular weight was determined by solving the equation that relates the excess scattered light, measured at several angles, to the concentration of solute and the weight-average molar mass. Trial runs were conducted on dextran (35–45 kDa) from Sigma prior to the experiments to test the system's performance.

2.4. Electrophoretic mobility measurements

To characterize the surface charge of the RNIP, RNIP-10AP, and guar gum-coated RNIP particles, their electrophoretic mobilities were measured using the ZetaPALS analyzer (Brookhaven Instruments Corp., Holtsville, NY) over a range of pH conditions in solutions of 1 and 10 mM NaCl concentrations. The 3 g/L stock dispersions of iron nanoparticles were fractionated by gravity and allowed to settle for 60 min, at which point only the stable particle fraction was collected from the supernatant to be used for the measurements. Ten electrophoretic mobility measurements were taken for each sample, and measurements were conducted for at least two independent samples under each pH condition.

2.5. Iron particle sizing, aggregation, and sedimentation

2.5.1. Particle sizing and aggregation experiments

DLS measurements were performed using a multi-detector light scattering unit (ALV-5000, Langen, Germany) which employs a Nd:vanadate laser (Verdi V2, Coherent, Santa Clara, CA) with a wavelength of 532 nm. The 3 g/L iron nanoparticle stock dispersions were fractionated by gravity and allowed to settle for 60 min before the supernatant was collected. The supernatant was subsequently diluted with water in the case of bare RNIP and RNIP-10AP

or with guar gum solutions to obtain guar gum-coated RNIP suspensions of different polymer concentrations, ranging from 0.05 to 1 g/L. For the aggregation experiments, the RNIP and guar gum concentrations used were 154 mg/L and 0.5 g/L, respectively. The final samples for DLS experiments were sonicated for 30 min using an Aquasonic Model 150T (VWR Scientific Products, Pennsylvania), just prior to the measurements. Each sample (2 mL) was introduced into a glass vial (Supelco, Bellefonte, PA) which had been soaked in cleaning solution (Extran MA01, Merck KGaA, Darmstadt, Germany), thoroughly rinsed with water, and oven-dried under dust-free conditions. For the aggregation experiments, a pre-measured amount of electrolyte stock solution was introduced into the vial containing the diluted nanoparticle suspension to induce aggregation. The vial was briefly vortexed (Mini Vortexer, Fisher Scientific) before being inserted into the toluene-filled quartz vat of the light scattering unit, and the DLS measurements were started immediately. The scattered light intensity was detected by a photodetector at a scattering angle of 90° , and each auto-correlation function was accumulated for 15 s. The intensity-weighted hydrodynamic radius of the aggregates was determined through second-order cumulant analysis (ALV software). The nanoparticle samples were left to aggregate over time periods of between 30 and 75 min.

2.5.2. Sedimentation experiments

For the sedimentation experiments, bare and guar gum-coated RNIP dispersions were prepared using the same protocol as for DLS experiments, but with a different dilution, yielding dispersions with a particle concentration of 385 mg/L. The dispersions were shaken but not sonicated prior to the experiment. All the dispersions contained nanoparticles of the same particle size at the beginning of the experiments. Therefore, the different sedimentation rates are only dependent on the aggregation process. The sedimentation profiles were obtained by measuring the optical density as a function of time at a wavelength of 508 nm (Hewlett-Packard Model 8453). The results were then analyzed following the approach presented by Phenrat et al. [24], which relates the sedimentation rates to different aggregation phases and particle sizes.

3. Results and discussion

3.1. General characteristics of iron nanoparticles

Representative TEM images of bare RNIP and RNIP-10AP aggregates are shown in Fig. 1. Primary particles are highly polydisperse and the size ranges from a few nanometers to about 200 nanometers. The shape of the particles is generally round and sometimes more rectangular. Previous studies claim the rectangular particles to be pure magnetite and the round ones to be Fe^0 with a shell of magnetite [29]. The size of the rectangular particles is generally larger than the round particles. No significant difference is observed between the bare RNIP and RNIP-10AP nanoparticles.

The observed aggregation of iron nanoparticles is due to the long-ranged magnetic attraction between iron nanoparticles [24]. Addition of polymers is needed for bare RNIP dispersions to offer the necessary repulsive forces to achieve stabilization. Considering the range and magnitude of magnetic forces, simple electrostatic repulsion is not likely to provide the required stabilization. As we discuss later, strong long-ranged steric repulsion is required for stabilization, which can be obtained through the utilization of high molecular weight polymers [4,32].

3.2. Relative stability of concentrated iron nanoparticles with various green polymers

Fig. 2 shows pictures of the glass vials containing the dispersions of RNIP coated with (a) guar gum, (b) potato starch, and

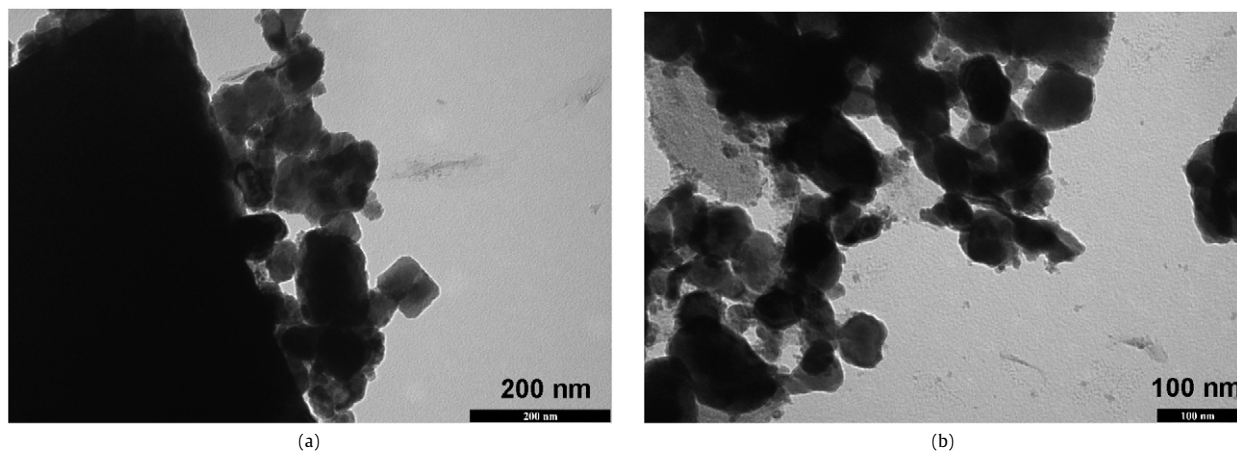


Fig. 1. Representative TEM images of (a) RNIP and (b) RNIP-10AP. RNIP and RNIP-10AP are polydisperse and have diameters ranging from a few nanometers to about 200 nm.

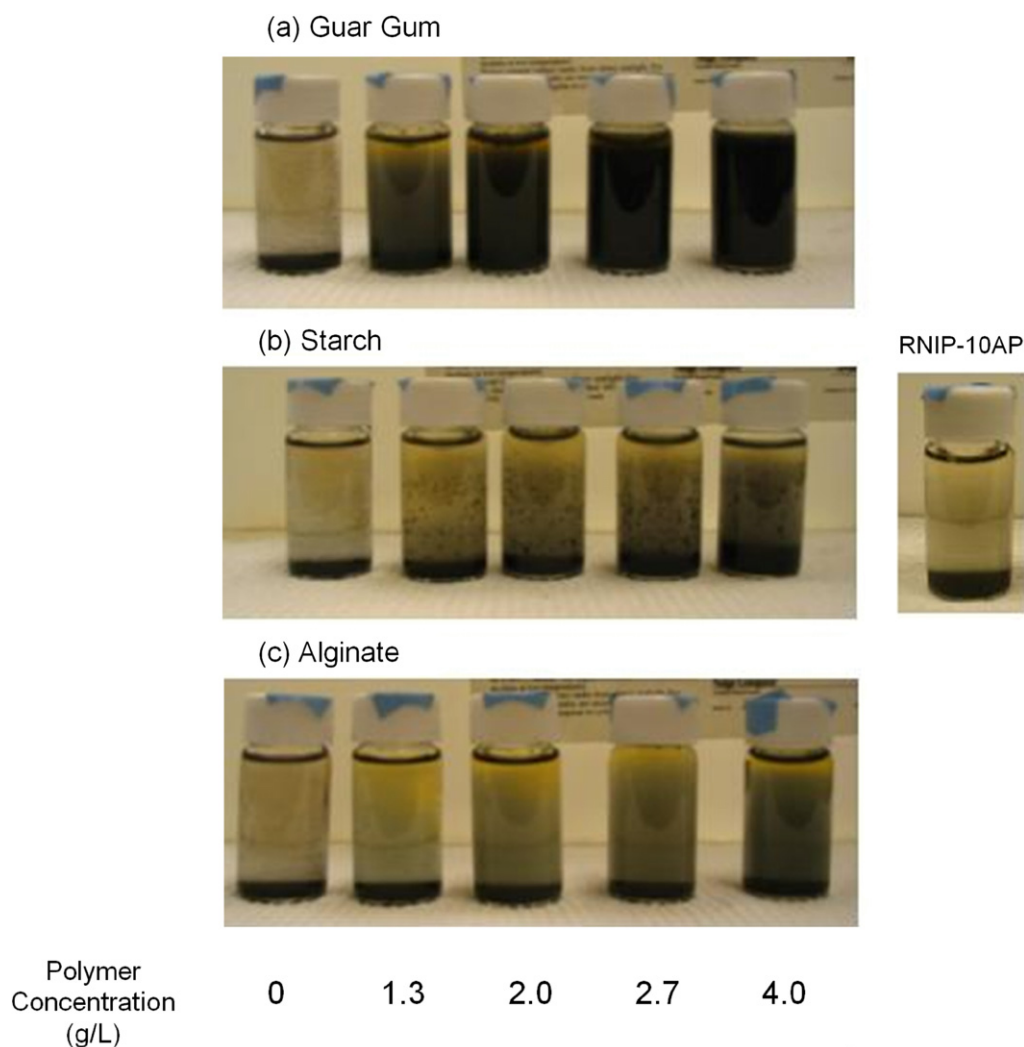


Fig. 2. Qualitative assessment of sedimentation rates of RNIP in solutions of different green polymers: (a) guar gum, (b) potato starch and (c) alginate. The samples were prepared at 1.5 g/L particle concentration in solutions of 1 mM NaCl and polymer concentrations of 0, 0.13, 0.2, 0.27 and 0.4 wt% at pH 7 ± 0.3 . The vial on the right is RNIP-10AP prepared at the same particle concentration (polymer concentration of 0.4 g/L). Pictures were taken after 1 h and sedimentation rates were evaluated qualitatively by observing the turbidity of the suspension.

(c) alginates, 1 h after initiation of the sedimentation test at 1 mM NaCl. At the start of the experiment, all test samples were uniformly black. After 1 h, the suspensions appear more uniformly dispersed with increasing polymer concentrations (from left to right: 0.0, 1.3, 2.0, 2.7 and 4.0 g/L). Significant differences in the

stabilizing effect of the polymers are observed. While all the vials containing potato starch and alginate-coated RNIP are clear even at the highest polymer concentration, the dispersions of guar gum-coated RNIP still appear dark, even for the lowest guar gum concentration. As the guar gum concentration is increased, the color

of the dispersions gets darker and becomes uniformly black for the vial with the highest guar gum content. This observation indicates that guar gum is much more effective than the other polymers in stabilizing the iron nanoparticles. Particles coated with guar gum remained in suspension for a few hours. The vial on the right shows a picture of the dispersion of RNIP-10AP diluted to obtain the same particle concentration as for the other vials, for comparison purposes. Given the results of this first qualitative screening, guar gum was chosen to be the most suitable polymer for stabilizing the iron nanoparticles. In the following sections, the stabilizing effects of guar gum are studied more extensively.

3.3. Guar gum solution properties

Guar gum is a natural nonionic water-soluble polysaccharide. It consists of a chain of (1 → 4)-linked β -D-mannopyranose units with α -D-galactopyranose units connected to the mannose backbone through (1 → 6) glycosidic linkages. Each unit contains nine hydroxyl groups, available for the formation of hydrogen bonds with other molecules [33]. Since guar gum does not have dissociable functional groups, it remains neutrally charged. It is also known that guar gum will degrade under extreme pH and high temperature conditions [34,35]. Because of its low cost, it is extensively used as a dispersing and stabilizing agent for industrial applications [36]. Guar gum is already being used to support the excavation walls for zero-valent iron permeable reactive barriers, where enzymes are then injected for its breakdown [2]. Recent studies have reported the effectiveness of guar gum in enhancing the sedimentation stability of magnetorheological fluids [37,38].

3.3.1. Titrated charge

Although guar gum is supposedly neutrally charged, the potentiometric titrations indicate that its acidity lies between 1.8 and 2.1 meq/g TOC. This value is low in comparison to that of other polysaccharides like alginates, which can go up to 11–12 meq/g TOC [39]. The acidity of guar gum solutions increases between pH 2 and 5, where it finally reaches a plateau (data not shown). This finding indicates the possible presence of carboxylic groups [40], which may be due to the presence of impurities in the commercial guar gum used.

3.3.2. Molecular weight

Fig. 3 shows the molecular weight distribution of the guar gum obtained from HPSEC-SLS. No significant difference exists between the sonicated and unsonicated samples indicating that sonication does not cause breakage of the polymers. The observed MW for both the samples lies between 800 and 5000 kDa. These results are consistent with previous observations [41] confirming that guar gum is a very high molecular weight polysaccharide, and is thus likely to provide steric stabilization of the iron nanoparticles.

3.3.3. Viscosity

A linear relationship between the viscosity and concentration of guar gum solutions is observed (Fig. 4). The viscosity increases as temperature decreases, and the changes in the viscosity are reversible as the temperature is restored. We also observed no significant effect of ionic strength and pH on the viscosity of the guar gum solution. Since the temperature, ionic strength, and pH of groundwater vary with location and fluctuate with time, the findings are important as they verify that the physical properties of guar gum do not change over the range of solution conditions tested.

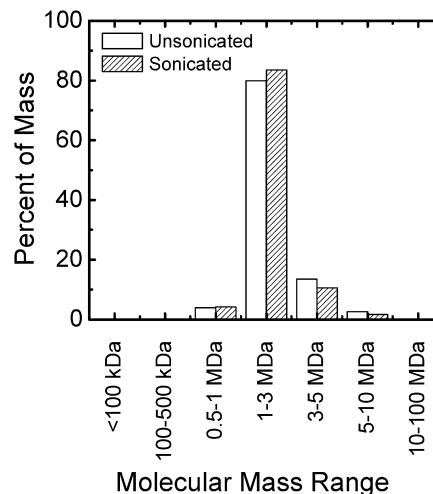


Fig. 3. High performance size exclusion chromatography analysis presenting the mass fractions within different molar mass ranges. Guar gum solutions were prepared at concentrations of 0.5 g/L before being filtered with a 0.45 μ m membrane filter. Both sonicated and unsonicated samples were analyzed for their respective mass fractions.

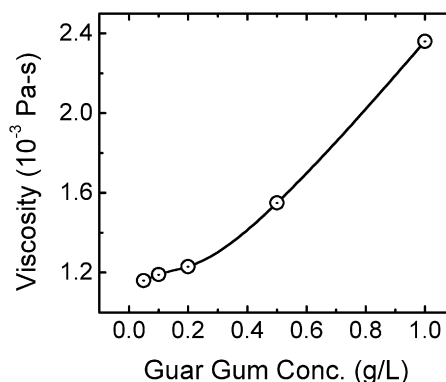


Fig. 4. Viscosity of guar gum solutions was measured over a range of guar gum concentrations at 25 ± 0.1 °C. The solutions were assumed to be Newtonian-like fluids. The viscosity of water is 0.89×10^{-3} Pa-s at 25 °C. Reported values were obtained at 1 mM NaCl and pH 7.0 ± 0.3 .

3.4. Characterization of iron nanoparticles in the presence of guar gum

3.4.1. Electrophoretic mobility

The electrophoretic mobilities (EPM) for RNIP and RNIP-10AP, as well as the guar gum-coated RNIP, are presented as a function of pH in Fig. 5. The RNIP consists of a core of Fe^0 and a shell of magnetite [29]. However, since the outer surface is not uniformly magnetite, the nanoparticles as a whole will exhibit electrokinetic properties of both the iron core and magnetite shell [8]. The isoelectric point (IEP) observed for RNIP is between pH 6.5 and 7 (Fig. 5a), which is close to that of pure magnetite (~ 6) [42]. As the electrolyte concentration is increased from 1 to 10 mM NaCl, the magnitudes of EPM decrease slightly across the pH range due to charge screening [43]. In comparison, the surface charge of RNIP-10AP is negative across the entire range of pH. This is because polyspartate adsorbed on the iron nanoparticles imparts a negative charge to the particle surface.

As for guar gum-coated nanoparticles, the surface charge appears to be slightly negative at alkaline pH, and the EPM becomes zero at pH below 4. This is consistent with the titration results, which implied the presence of small amounts of carboxyl groups. The profiles of EPM curves for different ionic strengths are identical as the outer surface charge of the guar gum-coated nanoparticles is extremely low. This behavior demonstrates again the ability

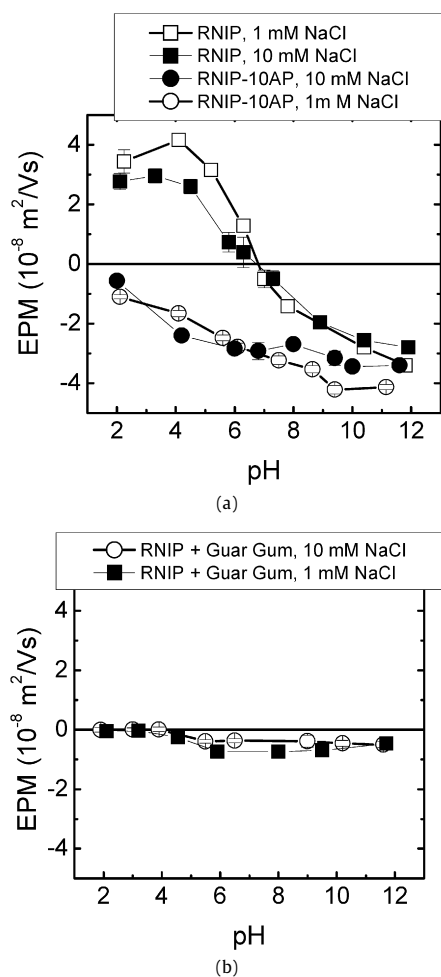


Fig. 5. Electrophoretic mobility (EPM) as a function of pH at 1 and 10 mM NaCl. (a) EPM of bare RNIP and RNIP-10AP. (b) EPM of RNIP in a solution of guar gum (0.5 g/L). Each data point represents the mean of at least a total of 10 measurements of at least two different samples at each pH, and the error bars represent standard deviations. Measurements were conducted at 25 °C.

of guar gum to adsorb on the nanoparticles. Because guar gum is almost neutrally charged, changing the ionic strength would have insignificant effect on the nanoparticle stability in the presence of this polymer.

3.4.2. Particle size

In order to study the effect of guar gum on RNIP particle size, DLS measurements were carried out on suspensions prepared at different particle and guar gum concentrations, as well as using different sonication protocols. First, we observed that increasing the particle concentration generally results in larger aggregate size since aggregation occurs more rapidly [45]. We also noticed that increasing the time period for sonication of the guar gum-coated RNIP reduces the aggregate size, suggesting that guar gum is able to prevent re-aggregation of flocs which have been broken apart during the sonication process. In Fig. 6, the effect of guar gum concentration on the aggregate hydrodynamic radius is presented. The iron nanoparticles were prepared at a concentration of 231 mg/L for these DLS measurements. The aggregate hydrodynamic radius decreases from over 300 nm to less than 200 nm as the guar gum concentration increases from 0.05 to 0.5 g/L. When the guar gum concentration is increased to 1 g/L, there is no further decrease in the hydrodynamic radius, indicating that the nanoparticle surface is likely to be saturated with the guar gum polymers at the concentration of 0.5 g/L. In comparison, the hydrodynamic ra-

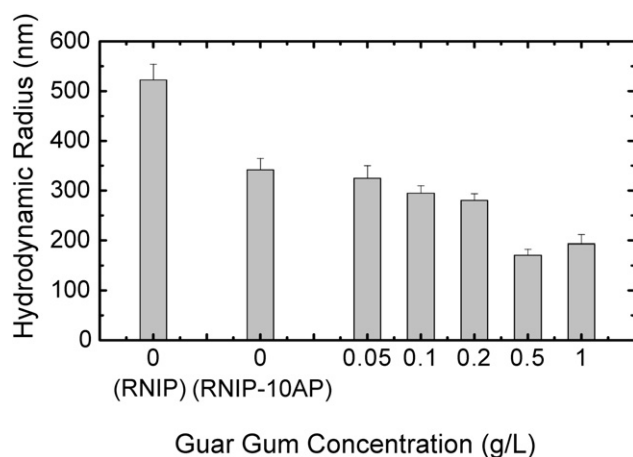


Fig. 6. Effect of guar gum concentration in solution on the average hydrodynamic radius of the guar gum-coated RNIP. All the measurements were carried out at pH 7.0 ± 0.3 in the absence of background electrolyte. 20 measurements were conducted under each condition to determine the average hydrodynamic radius. All measurements were conducted at 25 °C. Hydrodynamic radii of bare RNIP and RNIP-10AP were included for comparison purposes.

dius of bare RNIP aggregates at the same particle concentration is larger than 500 nm. As for RNIP-10AP, the hydrodynamic radius is ca. 350 nm, using a dispersion prepared following the same protocol as RNIP.

As already shown by Phenrat et al. [32] for other biopolymers, guar gum chains adsorbed on the nanoparticle surface seem to be able to provide strong steric repulsive forces that can oppose the attractive magnetic interactions. Calculations of the total interaction energy between primary particles show that a secondary energy minimum is present, with values of the same order of magnitude as the thermal energy, 1.5 kT, at 1 mM NaCl. Thus, only slight and reversible aggregation is expected in the presence of guar gum.

3.4.3. Aggregation

Fig. 7 presents representative aggregation profiles of bare and guar gum-coated RNIP, as obtained from the time-resolved DLS measurements. All aggregation experiments were conducted at nanoparticle and guar gum concentrations of 154 mg/L and 0.5 g/L, respectively. The initial hydrodynamic radii of the bare and guar gum-coated RNIP just before the addition of the electrolyte were approximately 360 and 160 nm, respectively (shown as dashed lines in Fig. 7).

Fig. 7a shows the aggregation profiles at an electrolyte concentration of 10 mM NaCl. As the electrical double layer is compressed, the hydrodynamic radius of bare RNIP increases from the initial radius of 360 nm to over 500 nm after 3000 s, reaching a plateau then after. This plateau does not indicate the ceasing of aggregation, but is most probably due to the sedimentation of the larger aggregates. A simple calculation invoking Stokes' law yields a sedimentation rate of approximately 0.27 mm/min for a spherical iron particle with a radius of 600 nm, which is high enough to affect the DLS measurement. In contrast, no aggregation is observed for the suspension containing guar gum as the steric repulsion by the adsorbed guar gum is not sensitive to salt concentration.

Fig. 7b presents the aggregation profiles at 0.5 M NaCl. We are not able to evaluate the very initial part of the profile for RNIP because significant aggregation has occurred during the time period between the introduction of the electrolyte and the first measurement, which accounts for approximately 25 s. The degree of charge screening at 0.5 M NaCl is much higher than at 10 mM NaCl, thus resulting in faster aggregation kinetics at the higher NaCl concentration. This is manifested through the increase of the hydrody-

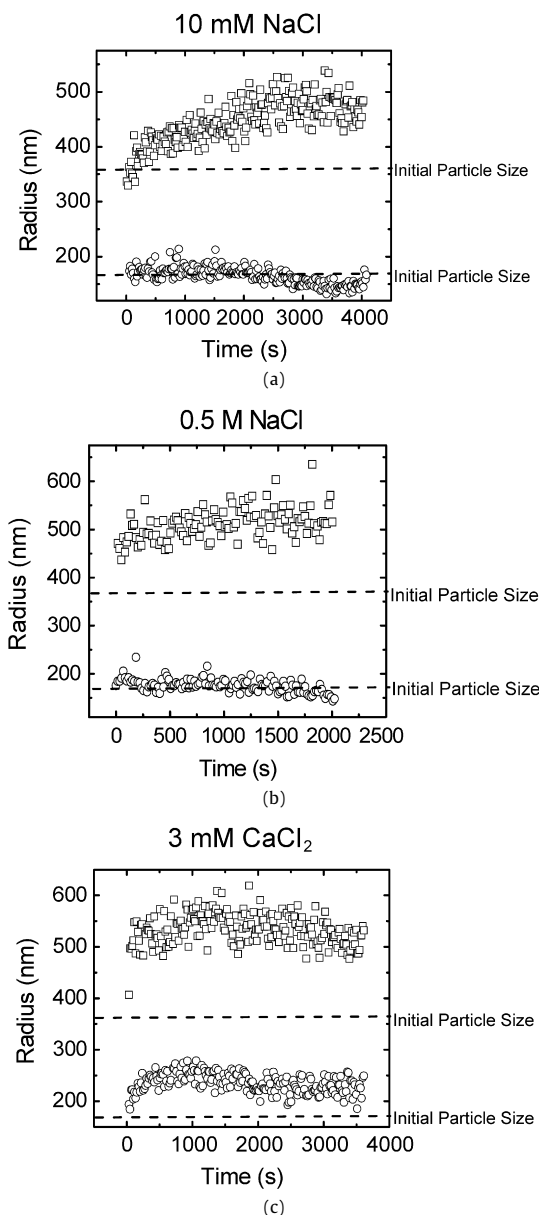


Fig. 7. Aggregation profiles of bare (□) and guar gum-coated (○) RNIP. All samples were prepared at pH 7.0 ± 0.3 . Aggregation was achieved using (a) 10 mM NaCl, (b) 0.5 M NaCl, and (c) 3 mM CaCl_2 . For all aggregation experiments, the concentrations of particles and guar gum employed are 154 mg/L and 0.5 g/L, respectively. Initial hydrodynamic radius for bare and guar gum-coated particles are 375.4 ± 19.2 nm and 162.8 ± 5.7 nm, respectively. All measurements were conducted at 25 °C.

dynamic radius to 550–600 nm in about 1000 s. Again, no significant aggregation is observed for guar gum-coated particles, even at this very high salt concentration of 0.5 M NaCl.

The aggregation profiles obtained in the presence of 3 mM CaCl_2 are presented in Fig. 7c. Significant aggregation is observed for RNIP, and the plateau, at a hydrodynamic radius of 550–600 nm, is reached in less than 1000 s. In the case of guar gum-coated RNIP, we detect only slight aggregation over the same period of time.

The above results indicate that guar gum is able to prevent aggregation through steric stabilization even in the presence of high NaCl concentrations. Slight aggregation occurs in the presence of calcium. This observation with calcium is likely due to polymer bridging through the formation of complexes between the few carboxyl functional groups on guar gum molecules and Ca^{2+}

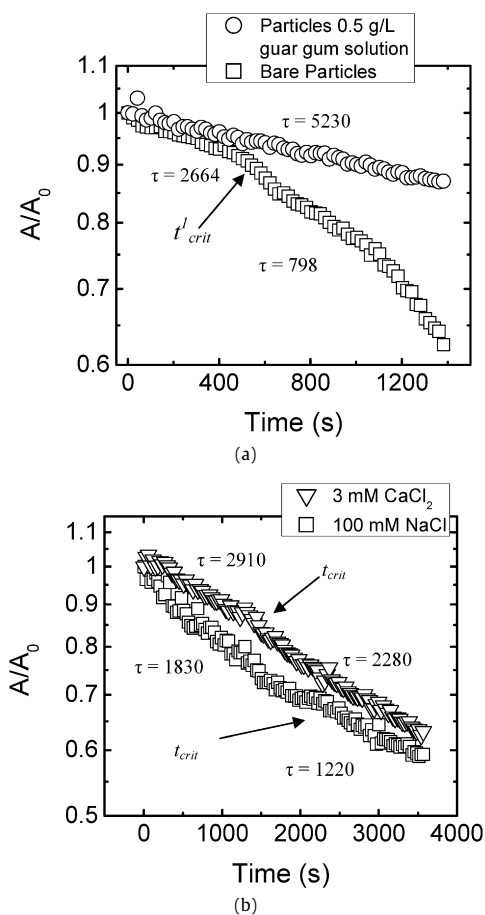


Fig. 8. Sedimentation curves of RNIP and RNIP in the presence of guar gum. The samples were prepared at pH 7 ± 0.3 . For all aggregation experiments, the concentrations of particles and guar gum employed are 385 mg/L and 0.5 g/L, respectively. All measurements were conducted at 25 °C. The samples of panel (a) were prepared in 1 mM NaCl electrolyte solutions, while the ones of panel (b) were prepared in 3 mM CaCl_2 and 100 mM NaCl electrolyte solutions, both in guar gum solutions.

ions [44,45]. However, this bridging mechanism will likely be less significant in groundwater due to the presence of a much larger background concentration of monovalent cations that exchange the calcium ions bound to the carboxyl groups on guar gum [45].

3.4.4. Sedimentation rates

Based on the observations made by Phenrat et al. [24], there are three phases characterizing the aggregation process of iron nanoparticles. Micrometer-sized aggregates form rapidly and subsequently link into chains. The effect of these mechanisms can be studied by monitoring the sedimentation rates of the RNIP dispersion. For more concentrated suspensions, sedimentation curves generally show different regions, related to the different phases of the aggregation process. Phenrat et al. suggest that at a certain time, defined as t_{crit} , the chain-like aggregate gel reaches a critical size which leads to more rapid sedimentation when compared to sedimentation that occurs at the initial stage of aggregation. This can be observed from sedimentation profiles measured using optical density (at 508 nm for the iron nanoparticles). The different sedimentation rates can be fitted by exponential decay. The characteristic time τ of the decay can then be related to the predicted average hydrodynamic radius of the aggregates, R_H , using [24]

$$\tau = \frac{9\eta(\beta - p_f)}{2g^2(\rho_s - \rho_l)^2 R_H^2} \quad (2)$$

Here, τ is obtained from the exponential decay curve fit $C = C_0 e^{-t/\tau}$, η is the solvent viscosity, β is a function of the perme-

ability of the fractal aggregate given by $\beta = 5 \times 10^9 (R_H)^{-1.5} \times 10^3$, p_f is the fluid pressure, ρ_s and ρ_l are the densities of solid component and liquid, respectively, and g is the gravitational acceleration. Using their approach, R_H has been found to be in good agreement with the ones obtained from DLS measurements [24].

Our experimental investigation was carried out on suspensions containing 385 mg/L of bare and guar gum-coated RNIP (Fig. 8). A/A_0 represents the absorbance normalized with the absorbance at the initial time of the experiment. In Fig. 8a, the sedimentation behavior of bare and guar gum-coated RNIP is compared in the presence of 1 mM NaCl. The sedimentation profile for bare RNIP shows three sedimentation regions, with the first t_{crit} , i.e., the time of formation of chain-like aggregates of a critical size, occurring after ca. 450 s. The first two regions are fitted with a decay curve, yielding R_H of $2.6 \pm 0.3 \mu\text{m}$ for the first region (0 to 450 s) and $9.3 \pm 0.8 \mu\text{m}$ for the second region (450 to 1050 s). No value of R_H was calculated for the third part as the mechanism for this sedimentation curve is still uncertain [24]. These calculated values generally agree with the observations of Phenrat et al. [24] at similar particle concentrations.

As for the guar gum-coated RNIP (Fig. 8a), we do not observe a change in the aggregation phase after 1300 s and the fitted decay curve results in a constant predicted hydrodynamic radius of $1.9 \pm 0.3 \mu\text{m}$. The larger dimension, compared to our DLS measurements presented earlier, is the result of both the use of a higher particle concentration and not sonicating the suspensions prior to the sedimentation experiments. Thus, guar gum appears to prevent aggregation at the tested conditions (1 mM NaCl). Fig. 8b shows the results of two guar gum-coated RNIP suspensions at a higher ionic strength (100 mM NaCl) and in the presence of calcium (3 mM CaCl_2). The different aggregation phases are only slightly discernible for both profiles. At a very particular level of detail, we can distinguish the phases and correlate them with their respective R_H . For the profile measured at 100 mM NaCl, the two radii are $6.9 \pm 0.4 \mu\text{m}$ and $10.6 \pm 0.6 \mu\text{m}$ after $t_{crit} = 2380$ s. At such an electrolyte concentration, which is higher than the one found in groundwater, chain formation in the presence of guar gum occurs rather late and the size of the chain-like aggregates is not dramatically larger than the size of the first phase aggregates. As for the curve obtained at 3 mM CaCl_2 , the first radius is calculated to be $4.0 \pm 0.4 \mu\text{m}$, and the second $5.4 \pm 0.7 \mu\text{m}$, after $t_{crit} = 1340$ s, indicating that even at high CaCl_2 concentrations, the guar gum-coated RNIP remain reasonably stable.

4. Concluding remarks

Surface modification via coating is crucial in achieving iron nanoparticle stabilization. In particular, steric stabilization is necessary to overcome the long-ranged attractive magnetic forces between the nanoparticles. This study investigated the effect of polymer coating on the aggregation and sedimentation behavior of iron nanoparticles, using commercially available, inexpensive, environmentally friendly green polymers. Guar gum would not present a risk to the environment and once introduced into the subsurface, it could also be used to enhance bioremediation. We have shown that guar gum, being a high molecular weight polysaccharide, is a suitable surface modifier. This polymer effectively coats the iron nanoparticles creating a slightly negatively charged layer. Iron nanoparticles that were stabilized by guar gum were much smaller compared to bare and polyaspartate-coated commercial particles. No aggregation was observed in the presence of guar gum even at very high ionic strength. Very slight aggregation was noted in the presence of 3 mM CaCl_2 , possibly due to gel bridging occurring between other polymers which may have contaminated the commercial guar gum employed for this study. Aggregation and sedimentation of guar gum-coated iron nanopar-

ticles are both significantly reduced, further verifying guar gum to be a suitable candidate to effectively stabilize iron nanoparticles.

Acknowledgments

This work was partially supported by the Project CIPE-C30 funded by Regione Piemonte, Italy. We also wish to thank Dr. Ewa Folta-Stogniew at the Biophysics Resource Keck Facility at Yale University for the high performance size exclusion chromatography analysis and Dr. Marc Pypaert at the Department of Cell Biology at the Yale University School of Medicine for the TEM imaging.

References

- [1] J.O. Sai, D.C. Anderson, Hazard. Waste Hazard. Mater. 9 (4) (1992) 317–330.
- [2] A. Di Molfetta, R. Sethi, Environ. Geol. 50 (33) (2006) 361–369.
- [3] Y. Yang, P.L. McCarty, Environ. Sci. Technol. 34 (14) (2000) 2979–2984.
- [4] N. Saleh, K. Sirk, Y.Q. Liu, T. Phenrat, B. Dufour, K. Matyjaszewski, R.D. Tilton, G.V. Lowry, Environ. Eng. Sci. 24 (1) (2007) 45–57.
- [5] W.X. Zhang, J. Nanopart. Res. 5 (3–4) (2003) 323–332.
- [6] C.B. Wang, W.X. Zhang, Environ. Sci. Technol. 31 (7) (1997) 2154–2156.
- [7] C.L. Geiger, C.A. Clausen, K.B. Brooks, C.C. Coon, L. Huntley, C. Filipek, R. DeVor, T.A. Krug, S. O'Hara, D. Major, J. Quinn, Abstr. Pap. Am. Chem. Soc. 225 (2003) U819.
- [8] Y.Q. Liu, Y.Q. Majetich, R.D. Tilton, D.S. Sholl, G.V. Lowry, Environ. Sci. Technol. 39 (5) (2005) 1338–1345.
- [9] H.L. Lien, W.X. Zhang, Colloids Surf. A Physicochem. Eng. Aspects 191 (1–2) (2001) 97–105.
- [10] S.H. Joo, A.J. Feitz, T.D. Waite, Environ. Sci. Technol. 38 (7) (2004) 2242–2247.
- [11] D.W. Elliott, J.S. Cao, W.X. Zhang, S.T. Spear, Abstr. Pap. Am. Chem. Soc. 225 (2003) U803.
- [12] G.V. Lowry, K.M. Johnson, Abstr. Pap. Am. Chem. Soc. 228 (2004) U607.
- [13] E. Hadnagy, K.H. Gardner, J.M. Spear, D. Aulisio, I. Calante, Abstr. Pap. Am. Chem. Soc. 228 (2004) U601.
- [14] M.C. Chang, H.Y. Shu, W.P. Hsieh, M.C. Wang, J. Air Waste Manage. Assoc. 55 (8) (2005) 1200–1207.
- [15] L. Li, M.H. Fan, R.C. Brown, J.H. Van Leeuwen, J.J. Wang, W.H. Wang, Y.H. Song, P.Y. Zhang, Crit. Rev. Environ. Sci. Technol. 36 (5) (2006) 405–431.
- [16] G. Jegadeesan, K. Mondal, S.B. Lalvani, Environ. Prog. 24 (3) (2005) 289–296.
- [17] S.R. Kanel, B. Manning, L. Charlet, H. Choi, Environ. Sci. Technol. 39 (5) (2005) 1291–1298.
- [18] S.M. Ponder, J.G. Darab, T.E. Mallouk, Environ. Sci. Technol. 34 (12) (2000) 2564–2569.
- [19] W.X. Zhang, Abstr. Pap. Am. Chem. Soc. 225 (2003) U961.
- [20] J. Quinn, C. Geiger, C. Clausen, K. Brooks, C. Coon, W.S. Yoon, A. Gavaskar, T. Holdsworth, S. O'Hara, T. Krug, D. Major, Environ. Sci. Technol. 39 (2005) 1309–1318.
- [21] S.R. Kanel, D. Nepal, B. Manning, H. Choi, J. Nanopart. Res. 9 (5) (2007) 725–735.
- [22] B. Schrick, B.W. Hydutsky, J.L. Blough, T.E. Mallouk, Chem. Mater. 16 (11) (2004) 2187–2193.
- [23] N. Saleh, T. Phenrat, K. Sirk, B. Dufour, J. Ok, T. Sarbu, K. Matyjaszewski, R.D. Tilton, G.V. Lowry, Nano Lett. 5 (12) (2005) 2489–2494.
- [24] T. Phenrat, N. Saleh, K. Sirk, R.D. Tilton, G.V. Lowry, Environ. Sci. Technol. 41 (1) (2007) 284–290.
- [25] P.M. Biesheuvel, J. Colloid Interface Sci. 275 (2004) 97–106.
- [26] B.W. Hydutsky, E.J. Mack, B.B. Beckerman, J.M. Skluzacek, T.E. Mallouk, Environ. Sci. Technol. 41 (18) (2007).
- [27] F. He, D.Y. Zhao, Environ. Sci. Technol. 39 (9) (2005) 3314–3320.
- [28] P.T. Anastas, J.B. Zimmerman, Environ. Sci. Technol. 37 (5) (2003) 94a–101a.
- [29] J.T. Nurmi, P.G. Tratnyek, V. Sarathy, D.R. Baer, J.E. Amonette, K. Pecher, C.M. Wang, J.C. Linehan, D.W. Matson, R.L. Penn, M.D. Driessen, Environ. Sci. Technol. 39 (5) (2005) 1221–1230.
- [30] X. Wang, B.I. Lee, L. Mann, Colloids Surf. A 202 (1) (2002) 71–80.
- [31] T.K. Corporation, Safety Data Sheets, 2005/03/17.
- [32] T. Phenrat, N. Saleh, K. Sirk, H.J. Kim, R.D. Tilton, G.V. Lowry, J. Nanopart. Res. 10 (5) (2008) 795–814.
- [33] J.M.W. Mackenzie, EGMJ (1980) 80–87.
- [34] Q. Wang, P.R. Ellis, S.B. Ross-Murphy, Food Hydrocolloids 14 (2) (2000) 129–134.
- [35] T.D. Bradley, A. Ball, S.E. Harding, J.R. Mitchell, Carbohydr. Polym. 10 (3) (1989) 205–214.
- [36] A.M. Goldstein, E.N. Alter, J.K. Seman, in: R.L. Whistler (Ed.), Industrial Gums, Polysaccharides and Their Derivatives, Academic press, New York, 1973, pp. 303–321.
- [37] C. Fang, B.Y. Zhao, L. Chen, Q. Wu, N. Liu, K.A. Hu, Smart Mater. Struct. 14 (1) (2005) N1–N5.

- [38] W.P. Wu, B.Y. Zhao, Q. Wu, L.S. Chen, K.A. Hu, *Smart Mater. Struct.* 15 (4) (2006) N94–N98.
- [39] W.S. Ang, M. Elimelech, *J. Membr. Sci.* 295 (2007) 83–92.
- [40] M.R. Collins, G.L. Amy, C. Steelink, *Environ. Sci. Technol.* 20 (1986) 1028–1032.
- [41] D.R. Picout, S.B. Ross-Murphy, N. Errington, S.E. Harding, *Biomacromolecules* 2 (4) (2001) 1301–1309.
- [42] Z.X. Sun, F.W. Su, W. Forsling, P.O. Samskog, *J. Colloid Interface Sci.* 197 (1) (1998) 151–159.
- [43] M. Elimelech, C.R. O'Melia, *Colloids Surf.* 44 (1990) 165–178.
- [44] K.L. Chen, S.E. Mylon, M. Elimelech, *Langmuir* 23 (2007) 5920–5928.
- [45] K.L. Chen, S.E. Mylon, M. Elimelech, *Environ. Sci. Technol.* 40 (2006) 1516–1523.